

# Finite-temperature magnetic properties of $\text{Sm}_2\text{Fe}_{17}\text{N}_x$ using an ab-initio effective spin model

<sup>1</sup>Shogo Yamashita, <sup>1</sup>Daiki Suzuki, <sup>1</sup>Takuya Yoshioka,

<sup>1,2</sup>Hiroki Tsuchiura, and <sup>3</sup>Pavel Novák

<sup>1</sup>Department of Applied Physics, Tohoku University, Aoba 6-6-05, Aoba-ku, Sendai 980-8579, Japan,

<sup>2</sup>Center for Spintronics Research Network, Tohoku University, Sendai 980-8577, Japan

<sup>3</sup>Institute of Physics, Academy of Sciences of the Czech Republic,

Cukrovarnická 10, 162 53 Praha 6, Czech Republic

(Dated: March 2, 2022)

In this study, we investigate the finite-temperature magnetic properties of  $\text{Sm}_2\text{Fe}_{17}\text{N}_x$  ( $x = 0, 3$ ) using an effective spin model constructed based on the information obtained by first-principles calculations. We find that assuming the plausible trivalent  $\text{Sm}^{3+}$  configuration results in a model that can satisfactorily describe the magnetization curves of  $\text{Sm}_2\text{Fe}_{17}\text{N}_3$ . By contrast, the model based on the divalent  $\text{Sm}^{2+}$  configuration is suitable to reproduce the magnetization curves of  $\text{Sm}_2\text{Fe}_{17}$ . These results expand the understanding of how electronic structure affects the magnetic properties of these compounds.

## I. INTRODUCTION

The  $\text{Sm}_2\text{Fe}_{17}\text{N}_x$  nitrides have unusual magnetic anisotropy properties. The system with  $x = 3$  is a commercially successful permanent magnet and is well known to exhibit stronger uniaxial magnetocrystalline anisotropy than  $\text{Nd}_2\text{Fe}_{14}\text{B}$ . In contrast, the system with  $x = 0$ , binary  $\text{Sm}_2\text{Fe}_{17}$ , has weak planar anisotropy, and a recent experiment has revealed that the magnetization orientation slightly deviates from the basal plane by about  $10^\circ$  at low temperatures<sup>1</sup>. Because the iron sublattice of this system is expected to have planar magnetic anisotropy analogous to  $\text{Y}_2\text{Fe}_{17}$ , this observation indicates that the local magnetic anisotropy due to the Sm ions is uniaxial but comparatively weak in  $\text{Sm}_2\text{Fe}_{17}$ . Thus, the nitrogenation process sensitively changes the electronic states around the Sm ions, resulting in a sign change of the magnetocrystalline anisotropy.

Several efforts have been made to theoretically clarify the electronic states of  $\text{Sm}_2\text{Fe}_{17}\text{N}_x$  based on first-principles calculations<sup>2–5,8</sup>. Because modern first-principles calculations still do not treat 4f electrons properly, some additional treatment such as the so-called open core method, the local spin density approximation with Hubbard correction (LSDA+ $U$ ), or the self-interaction correction (SIC) is needed to evaluate the magnetic anisotropy of these systems. Steinbeck *et al.*<sup>3</sup> calculated the 4f crystal field parameters (CFPs) for the Sm ions based on the open core method, assuming a plausible trivalent  $\text{Sm}^{3+}$  configuration. They found that the second-order CFP  $A_2^0$ , which dominates the local magnetic anisotropy of Sm, is enhanced in amplitude by nitrogenation. Knyazev *et al.*<sup>4</sup> calculated the electronic structure and optical properties of  $\text{Sm}_2\text{Fe}_{17}$  and  $\text{Tm}_2\text{Fe}_{17}$  using the LSDA+ $U$  method. The calculated total magnetic moment including the orbital correction to the contribution from 4f electrons is in good agreement with the experimentally measured value<sup>9</sup>. However, they did not discuss the magnetic anisotropy of the sys-

tems. Pandey *et al.*<sup>5</sup> calculated the magnetocrystalline anisotropy energy of  $\text{Sm}_2\text{Fe}_{17}$  and  $\text{Sm}_2\text{Fe}_{17}\text{N}_3$ . The predicted directions of magnetocrystalline anisotropy for  $\text{Sm}_2\text{Fe}_{17}$  and  $\text{Sm}_2\text{Fe}_{17}\text{N}_3$  are in good agreement with the experimental observations. However, the calculated total moments are smaller than the experimentally measured values<sup>6,7</sup>. According to their results, the calculated spin magnetic moments of the Sm ions are close to that of trivalent  $\text{Sm}^{3+}$ . Recently, Ogura *et al.*<sup>8</sup> carried out self-consistent Korringa–Kohn–Rostoker coherent potential approximation (KKR-CPA) calculations with a SIC treatment, and confirmed that the uniaxial magnetocrystalline anisotropy increases with increasing nitrogen content  $x$ . In addition, they claimed that the number of f electrons of each Sm ion is about 6; that is, a divalent  $\text{Sm}^{2+}$  configuration is realized, regardless of  $x$ . This result is quite intriguing because it has been widely believed that the Sm ions have trivalent electronic states, as claimed in several X-ray absorption spectroscopy (XAS) experiments<sup>10</sup>.

We notice that these theoretical studies except the work of Pandey *et al.* concluded uniaxial magnetocrystalline anisotropy not only for  $\text{Sm}_2\text{Fe}_{17}\text{N}_3$ , but also for  $\text{Sm}_2\text{Fe}_{17}$ , which is inconsistent with the reported experimental observations. It should be also noted here that the KKR-CPA with SIC calculations showed that the uniaxial magnetic anisotropy of  $\text{Sm}_2\text{Fe}_{17}$  is fairly small. This is intuitively understandable because the 4f electron clouds of divalent  $\text{Sm}^{2+}$  should be more spherical than those of trivalent  $\text{Sm}^{3+}$ , resulting in a weaker uniaxial local magnetic anisotropy. Although information about the electronic states of Sm is quite important to understand the magnetic properties, in particular, the magnetocrystalline anisotropy, it is difficult to extend the conclusions of the previous studies by using the first-principles calculation method itself. Therefore, we instead focus on the finite-temperature magnetic properties of the systems. We construct a single-ion model, which has long been used to describe phenomenologically the magnetic properties of rare-earth based materials, but base it on

first-principles calculations. The necessary information to construct the model is as follows: the magnetic moments of each ion, the exchange field acting on the 4f electrons, and the CFPs. Once we construct the model, including the crystal-field Hamiltonian, we can compute the magnetic anisotropy due to the rare-earth ions for arbitrary temperatures in the standard statistical mechanical way. For this purpose, the most suitable way to treat the 4f electrons in first-principles calculations is the open core method because we can easily control the electronic structure and valency of the Sm ions.

In this study, we investigate the magnetization curves of  $\text{Sm}_2\text{Fe}_{17}\text{N}_x$  ( $x = 0, 3$ ) for several temperatures using the single-ion model based on first-principles calculations. We prepare the model in two ways: (1) assuming trivalent Sm ions, and (2) assuming divalent Sm ions. We show the differences between the magnetization curves obtained by (1) and (2), and discuss which valency and electronic configurations plausibly describe the experimentally obtained finite-temperature magnetic properties.

## II. ELECTRONIC STRUCTURE CALCULATIONS AND MODEL CONSTRUCTION

We use the single-ion Hamiltonian<sup>11–15</sup> to describe the finite-temperature magnetic properties of  $\text{Sm}_2\text{Fe}_{17}\text{N}_x$  ( $x = 0, 3$ ). The Hamiltonian of the  $i$ -th Sm ion is given as

$$\mathcal{H}(i) = \lambda \mathbf{L}_{4f} \cdot \mathbf{S}_{4f} + 2\mathbf{H}_m(T) \cdot \mathbf{S}_{4f} + \mathcal{H}_{\text{CEF}}(i) + (\mathbf{L}_{4f} + 2\mathbf{S}_{4f}) \cdot \mathbf{H}_{\text{ex}}, \quad (1)$$

where  $\mathbf{L}_{4f}$  and  $\mathbf{S}_{4f}$  are the total spin and total angular momentum operators,  $\lambda$  is the spin-orbit coupling constant of the 4f shell,  $\mathbf{H}_{\text{ex}}$  is the external magnetic field, and  $\mathbf{H}_m(T)$  is the exchange mean-field acting on the spin components of 4f electrons. The crystal-field Hamiltonian  $\mathcal{H}_{\text{CEF}}(i)$  is expressed in terms of the tensor operator method as follows<sup>12,13</sup>:

$$\begin{aligned} \mathcal{H}_{\text{CEF}}(i) = & A_2^0(i) \sum_j r_j^2 2U_2^0(\theta_j, \phi_j) \\ & + A_4^0(i) \sum_j r_j^4 8U_4^0(\theta_j, \phi_j) + A_6^0(i) \sum_j r_j^6 16U_6^0(\theta_j, \phi_j) \\ & + A_6^6(i) \sum_j r_j^6 \left( \frac{1}{231} \right)^{\frac{1}{2}} [U_6^6(\theta_j, \phi_j) + U_6^{-6}(\theta_j, \phi_j)], \end{aligned} \quad (2)$$

where  $A_l^m(i)$  are the CFPs at the  $i$ -th rare-earth ion site. In this work, assuming that all sites are equivalent, we neglect contributions from  $A_4^3(i)$  and  $A_6^3(i)$ . The tensor operator  $U_l^m$  is given by

$$U_l^m(\theta_j, \phi_j) = \sqrt{\frac{4\pi}{2l+1}} Y_{l,m}(\theta_j, \phi_j), \quad (3)$$

TABLE I. The reduced matrix elements<sup>13</sup> used in our calculations.

	$\langle L    U_2    L \rangle$	$\langle L    U_4    L \rangle$	$\langle L    U_6    L \rangle$
$\text{Sm}^{3+}$	$\frac{1}{3} \left( \frac{2 \cdot 11 \cdot 13}{15} \right)^{\frac{1}{2}}$	$\frac{2}{3} \left( \frac{2 \cdot 13}{11} \right)^{\frac{1}{2}}$	$-10 \left( \frac{5 \cdot 17}{3 \cdot 11 \cdot 13} \right)^{\frac{1}{2}}$
$\text{Sm}^{2+a}$	$2 \left( \frac{7}{15} \right)^{\frac{1}{2}}$	$-\left( \frac{14}{11} \right)^{\frac{1}{2}}$	$10 \left( \frac{7}{3 \cdot 11 \cdot 13} \right)^{\frac{1}{2}}$

<sup>a</sup> For  $\text{Sm}^{2+}$  we show the values of  $\text{Eu}^{3+}$ .

where  $Y_{l,m}$  is the spherical harmonics function. Matrix elements of  $\sum_j r_j^l U_l^m(\theta_j, \phi_j)$  are expressed using 3-j and 6-j symbols as follows<sup>12,13</sup>:

$$\begin{aligned} & \langle J, J_z, L, S | \sum_j r_j^l U_l^m(\theta_j, \phi_j) | J', J'_z, L, S \rangle \\ & = (-1)^{(L+S-J_z+J+J')} \sqrt{(2J+1)(2J'+1)} \\ & \times \begin{pmatrix} J & J' & l \\ -J_z & J'_z & m \end{pmatrix} \begin{Bmatrix} L & L & l \\ J & J' & S \end{Bmatrix} \langle L || U_l || L \rangle \langle r^l \rangle, \end{aligned} \quad (4)$$

where  $\langle L || U_l || L \rangle$  is the appropriate set of reduced matrix elements given in Table I. We note that  $J$  multiplets are taken into account up to the fifth excited state in this calculation. We use  $L = 5$  and  $S = \frac{5}{2}$  for  $\text{Sm}^{3+}$ , and  $L = 3$  and  $S = 3$  for  $\text{Sm}^{2+}$ .

Once we have set the Hamiltonian for the  $i$ -th Sm ion, we can obtain the free energy for the 4f partial system based on the statistical mechanical procedure, as

$$F(i) = -k_B T \ln \text{Tr} \exp \left[ -\frac{\mathcal{H}(i)}{k_B T} \right]. \quad (5)$$

This single-ion Hamiltonian has a quite long history, and in the early days of the study of rare-earth-based permanent magnets, the model parameters such as  $|\mathbf{H}_m(0)|$  and  $A_l^m$  were determined by multi-parameter fitting calculations to the experimental magnetization curves of single crystals<sup>13</sup>. Now, we can determine these parameters based on the information of the electronic states of the systems using first-principles calculations. Recently, we have confirmed that this procedure successfully describes the observed magnetization curves and the temperature dependences of anisotropy constants of  $R_2\text{Fe}_{14}\text{B}$  ( $R = \text{Dy, Ho}$ )<sup>16</sup> and  $\text{SmFe}_{12}$ <sup>17</sup>.

We use the first-principles calculations method to determine the CFPs. Once the electronic state calculations are completed, we can compute the CFPs  $A_l^m \langle r^l \rangle$  in Eq. (2) based on the well-known formula<sup>18–20</sup>

$$A_l^m \langle r^l \rangle = a_{lm} \int_0^{R_{\text{MT}}} dr r^2 |R_{4f}(r)|^2 V_l^m(r), \quad (6)$$

where  $V_l^m(r)$  is the component of the partial wave expansion of the total Coulomb potential of the rare-earth ions within the atomic sphere of radius  $R_{\text{MT}}$ .  $a_{lm}$  are numerical factors, specifically,  $a_{20} = \frac{1}{4} \sqrt{\frac{5}{\pi}}$ ,  $a_{40} = \frac{3}{16} \sqrt{\frac{1}{\pi}}$ ,  $a_{60} = \frac{1}{32} \sqrt{\frac{13}{\pi}}$ ,  $a_{66} = \frac{231}{64} \sqrt{\frac{26}{231\pi}}$ , and  $R_{4f}(r)$  is the radial shape of the localized 4f charge density of the rare-earth ions. We can directly obtain  $V_l^m(r)$  from the

TABLE II. The anisotropy constants  $K_{\text{Fe}}$  [K] per single Fe atom.<sup>1,22,23</sup>

	4.2K	300K
$\text{Sm}_2\text{Fe}_{17}$	-4.14	-0.45
$\text{Sm}_2\text{Fe}_{17}\text{N}_3$	-2.60	-1.30

density functional theory (DFT) potential calculated by WIEN2k<sup>21</sup>. Moreover, to simulate the localized 4f electronic states in the system, we use the *classical* open core method, in which we switch off the hybridization between 4f and valence 5d and 6p states and treat the 4f states in the spherical part of the potential as atomic-like core states<sup>18</sup>. Thus, the function  $R_{4f}(r)$  in Eq. (6) can be obtained by performing separate atomic calculations of the electronic structure of an isolated rare-earth atom. The details of the calculations are provided in previous studies<sup>18–20</sup>.

Using the polar coordinates  $(\theta, \phi)$ , which are the zenith and azimuth angles defined with the  $c$ -axis as the  $z$ -axis, the total free energy of the system is given by

$$F(\mathbf{H}_{\text{ex}}, H_{\text{m}}(T), T, \theta, \phi) = \sum_{i=1}^{N_{\text{R}}} F(i) + N_{\text{Fe}} K_{\text{Fe}}(T) \sin^2 \theta - \mathbf{M}_{\text{Fe}}(T) \cdot \mathbf{H}_{\text{ex}}, \quad (7)$$

where  $N_{\text{R}}$  and  $N_{\text{Fe}}$  are the numbers of Sm ions and Fe ions, respectively;  $H_{\text{m}}(T) = |\mathbf{H}_{\text{m}}(T)|$ ; and  $K_{\text{Fe}}(T)$  is the anisotropy constant of Fe per atom given in Table II. The same notation is used as in Eq. (1). The temperature dependence of  $\mathbf{M}_{\text{Fe}}(T)$  is described by the Kuz'min formula as follows<sup>24</sup>:

$$\mathbf{M}_{\text{Fe}}(T) = \mathbf{M}_{\text{Fe}}(0) \left[ 1 - s \left( \frac{T}{T_{\text{c}}} \right)^{\frac{3}{2}} - (1-s) \left( \frac{T}{T_{\text{c}}} \right)^p \right]^{\frac{1}{3}} \quad (8)$$

where  $\mathbf{M}_{\text{Fe}}(0)$  is the total magnetic moment of the system except the magnetic moment of the Sm ions. The calculated results of  $\mathbf{M}_{\text{Fe}}(0)$  are summarized in Table III. The temperature dependence of  $\mathbf{H}_{\text{m}}(T)$  is also described by the Kuz'min formula<sup>24</sup>:

$$\mathbf{H}_{\text{m}}(T) = \mathbf{H}_{\text{m}}(0) \left[ 1 - s \left( \frac{T}{T_{\text{c}}} \right)^{\frac{3}{2}} - (1-s) \left( \frac{T}{T_{\text{c}}} \right)^p \right]^{\frac{1}{3}}. \quad (9)$$

In this system, we use  $s = 0.7$  and  $p = 5/2$  given by Kuz'min<sup>24</sup>. The Curie temperatures  $T_{\text{c}}$  of  $\text{Sm}_2\text{Fe}_{17}$  and  $\text{Sm}_2\text{Fe}_{17}\text{N}_3$  are 380K<sup>1</sup> and 752K<sup>25</sup>, respectively. Calculating Eq. (7) for given  $(\theta, \phi)$ , we obtain the angular dependence of the total free energy. We note that the directions of  $\mathbf{H}_{\text{m}}(T)$  and  $\mathbf{M}_{\text{Fe}}(T)$  are anti-parallel. The equilibrium directions of  $\mathbf{M}_{\text{Fe}}(T)$  and  $\mathbf{H}_{\text{m}}(T)$  are evaluated using the minimum point of the total free energy of

the system. We numerically examine all the angles  $(\theta, \phi)$  that correlate with the energy minimum point. These angles determine the direction of the Fe sublattice magnetization in equilibrium. The finite-temperature magnetic moment of the  $i$ -th Sm ion  $\mathbf{M}_{\text{R}}^i(T)$  is given by

$$\mathbf{M}_{\text{R}}^i(T) = - \sum_{\mathbf{s}} \langle i, \mathbf{s} | \mathbf{L}_{4f} + 2\mathbf{S}_{4f} | i, \mathbf{s} \rangle e^{-E_{\mathbf{s}}(i)/k_{\text{B}}T} / Z(i), \quad (10)$$

$$Z(i) = \sum_{\mathbf{s}} e^{-\frac{E_{\mathbf{s}}(i)}{k_{\text{B}}T}}, \quad (11)$$

where  $E_{\mathbf{s}}(i)$  and  $|i, \mathbf{s}\rangle$  are an eigenvalue and eigenvector, respectively, of the following equation:

$$\mathcal{H}(i) |i, \mathbf{s}\rangle = E_{\mathbf{s}}(i) |i, \mathbf{s}\rangle. \quad (12)$$

The total magnetic moment of the system  $\mathbf{M}(T)$  is represented by

$$\mathbf{M}(T) = \sum_i \mathbf{M}_{\text{R}}^i(T) + \mathbf{M}_{\text{Fe}}(T). \quad (13)$$

We plot the magnetization curves of both compounds at 4.2K and 300K because the anisotropy constants of Fe summarized in Table II are measured at a specific temperature. In order to calculate the magnetic anisotropy constants  $K_1(T)$  and  $K_2(T)$ , we assume the following expansion:

$$F(\mathbf{H}_{\text{ex}}, H_{\text{m}}(T), T, \theta, \phi) - N_{\text{Fe}} K_{\text{Fe}}(T) \sin^2 \theta = K_1(T) \sin^2 \theta + K_2(T) \sin^4 \theta + \dots \quad (14)$$

We use Maclaurin's expansion to obtain the anisotropy constants as follows<sup>26</sup>:

$$K_1(T) = \frac{1}{2} \frac{\partial^2 F(0, H_{\text{m}}(T), T, \theta, \phi)}{\partial \theta^2} \Big|_{\theta=0}, \quad (15)$$

$$K_2(T) = \frac{1}{3} K_1(T) + \frac{1}{24} \frac{\partial^4 F(0, H_{\text{m}}(T), T, \theta, \phi)}{\partial \theta^4} \Big|_{\theta=0}. \quad (16)$$

We note that the magnetic anisotropy of Fe is not included in  $K_1(T)$  and  $K_2(T)$  in this work, because we cannot treat the temperature dependence of the magnetic anisotropy of Fe theoretically.

We calculate  $|\mathbf{H}_{\text{m}}(0)|$  in accordance with the method of Brooks *et al.*<sup>27</sup>. We summarize the model parameters, including CFPs,  $H_{\text{m}}(0)$ , and  $\lambda$ , in Table IV.

For the computation of the necessary parameters for the single-ion model, we use the WIEN2k code (Version 16.1), adopting the generalized-gradient approximation form for the exchange-correlation functional. Here, the lattice constants of the unit cell are set to the experimental values of  $a = b = 8.557\text{\AA}$  and  $c = 12.448\text{\AA}$  for  $\text{Sm}_2\text{Fe}_{17}$ <sup>28</sup>, and  $a = b = 8.7206\text{\AA}$  and  $c = 12.63445\text{\AA}$

for  $\text{Sm}_2\text{Fe}_{17}\text{N}_3$ <sup>22</sup>. The space group of both compounds is  $R\bar{3}m$  (No. 166). The atomic sphere radii are taken to be 3.0, 1.96, and 1.6 a.u. for Sm, Fe, and N, respectively. Spin-orbit coupling is not considered in our first-principles calculations. The number of basis functions of  $\text{Sm}_2\text{Fe}_{17}$  and  $\text{Sm}_2\text{Fe}_{17}\text{N}_3$  are taken to be 1609 and 2934, respectively, and  $4 \times 4 \times 4$   $k$  points are sampled in the Brillouin zone.  $RK_{\text{MAX}}$  is taken to be 7.0 in our calculations. Crystal structure and non-equivalent atomic positions of  $\text{Sm}_2\text{Fe}_{17}\text{N}_3$  and  $\text{Sm}_2\text{Fe}_{17}$  are shown in FIG. 1.

### III. RESULTS AND DISCUSSION

#### A. Electronic structure

We explain the calculated electronic structure for  $\text{Sm}_2\text{Fe}_{17}$  and  $\text{Sm}_2\text{Fe}_{17}\text{N}_3$ . We show the spin magnetic moments of the Fe ions on each site, the total spin magnetic moments in the cell except the contribution from the Sm spin magnetic moments, and the total magnetic moments in the unit cell at 0K in Table III, for comparison with the results of previous studies<sup>3,8</sup>. The total magnetic moments in the unit cell are calculated by Eq. (1) and Eq. (13), because the magnetic moments of the Sm ions contain the contribution from the orbital magnetic moments of 4f orbitals. The nearest neighbor sites for the Sm ions in  $\text{Sm}_2\text{Fe}_{17}$  are 18f sites. In contrast, the nearest neighbor sites for the Sm ions in  $\text{Sm}_2\text{Fe}_{17}\text{N}_3$  are 18h sites<sup>3,22</sup>. The difference of the valency does not affect the spin magnetic moments of each site drastically. We find that the nitrogeation causes the enhancement of the magnetic moments at 9d sites and reduction of those at 18f sites in both valency. Similar effects are discussed in Ogura *et al.* However, no enhancement of magnetic moments at 6c sites was found in this work. We note that the magnetic moments of each Fe site in trivalent  $\text{Sm}_2\text{Fe}_{17}$  are quite different from the results of Steinbeck *et al.*, especially on 9d sites, and the magnetic moments of each Fe site in trivalent  $\text{Sm}_2\text{Fe}_{17}\text{N}_3$  are similar to their results except that of 6c sites<sup>3</sup>. For the trivalent configuration, we can see that the total magnetic moments of Sm ions in  $\text{Sm}_2\text{Fe}_{17}$  and  $\text{Sm}_2\text{Fe}_{17}\text{N}_3$  are  $0.48\mu_B$  and  $0.41\mu_B$ , respectively. In contrast, for the divalent configuration, we can see the negative contribution; the total magnetic moments of Sm ions are  $-2.70\mu_B$  and  $-2.68\mu_B$  for  $\text{Sm}_2\text{Fe}_{17}$  and  $\text{Sm}_2\text{Fe}_{17}\text{N}_3$ , respectively. The comparison of the calculated total magnetic moment at low temperature with experimentally measured values are discussed in sections III. B and III. C. Next, we show the CFPs  $A_l^m\langle r^l \rangle$  calculated by Eq. (6) in Table IV. We can see that the CFPs  $A_l^m\langle r^l \rangle$  of  $\text{Sm}_2\text{Fe}_{17}\text{N}_3$  do not change drastically, except  $A_2^0\langle r^2 \rangle$ , when we change the valency of the Sm ions. We also note that the values of  $A_2^0\langle r^2 \rangle$  for  $\text{Sm}_2\text{Fe}_{17}\text{N}_3$  are the largest regardless of the its valency. This implies that  $\text{Sm}_2\text{Fe}_{17}\text{N}_3$  shows uniaxial anisotropy, regardless of the valency of the Sm ions. However, we can see that

TABLE III. Spin magnetic moments in unit  $\mu_B$  of each Fe ion, total spin magnetic moment in the cell except the contribution from the Sm, and total magnetic moment per unit cell calculated by our effective single-ion model for each valency, with comparison to previous works<sup>3,8</sup>.

	Valency	6c	9d	18f	18h	$M_{\text{Fe}}(0)$	Total
Present work							
$\text{Sm}_2\text{Fe}_{17}$	$\text{Sm}^{3+}$	2.67	2.21	2.49	2.39	39.72	40.19
	$\text{Sm}^{2+}$	2.71	2.20	2.50	2.42	41.06	35.66
Present work							
$\text{Sm}_2\text{Fe}_{17}\text{N}_3$	$\text{Sm}^{3+}$	2.65	2.48	2.18	2.36	38.80	39.41
	$\text{Sm}^{2+}$	2.69	2.49	2.10	2.40	38.96	33.61
Steinbeck <i>et al.</i> <sup>3 a</sup>							
$\text{Sm}_2\text{Fe}_{17}$	$\text{Sm}^{3+}$	2.41	1.57	2.22	2.02	—	—
$\text{Sm}_2\text{Fe}_{17}\text{N}_3$	$\text{Sm}^{3+}$	2.36	2.45	2.13	2.42	—	—
Ogura <i>et al.</i> <sup>8 b</sup>							
$\text{Sm}_2\text{Fe}_{17}$	—	2.53	2.15	2.42	2.17	—	—
$\text{Sm}_2\text{Fe}_{17}\text{N}_3$	—	2.92	2.84	2.14	2.12	—	—

- <sup>a</sup> The Sm ions are treated as trivalent in a similar method with the open core method.  
<sup>b</sup> They did not use the open core method, thus the valency of the Sm ions is not shown. We extracted the values of magnetic moments from Fig. 2 of Ogura *et al.*<sup>8</sup>

the CFP  $A_2^0\langle r^2 \rangle$  of  $\text{Sm}_2\text{Fe}_{17}$  is quite different in trivalent and divalent results.  $A_2^0\langle r^2 \rangle$  in the trivalent result is the largest among the CFPs; however,  $A_2^0\langle r^2 \rangle$  in the divalent result is quite small compared with the others. This implies that the difference of the valency of the Sm ions causes the change of the anisotropy of the system.

#### B. Magnetization curves of $\text{Sm}_2\text{Fe}_{17}\text{N}_3$

First, we look at the magnetization curves of  $\text{Sm}_2\text{Fe}_{17}\text{N}_3$  calculated by the effective spin model. FIG. 2 (a) shows the magnetization curves along the [001] and [100] directions at  $T = 4.2\text{K}$ , obtained by using the effective spin model with the trivalent  $\text{Sm}^{3+}$  (red) and the divalent  $\text{Sm}^{2+}$  (black). The experimental results for  $\text{Sm}_2\text{Fe}_{17}\text{N}_{3.1}$  reported by Koyama *et al.*<sup>25</sup> are indicated by solid curves in FIG. 2 (a). We can clearly see that the [001] direction is the easy axis of this system, regardless of the valency of the Sm ions. However, as we noted in the section III. A, the saturation magnetizations  $M_s$  at low temperature for  $\text{Sm}^{3+}$  and  $\text{Sm}^{2+}$  are clearly different. We also notice here that the results for the trivalent model in FIG. 2 (a) satisfactorily reproduce the experimentally observed magnetization curves. Thus, we can conclude that the  $\text{Sm}^{3+}$  electronic configuration is realized in  $\text{Sm}_2\text{Fe}_{17}\text{N}_3$  compounds.

The magnetization curves of  $\text{Sm}_2\text{Fe}_{17}\text{N}_3$  at  $T = 300\text{K}$

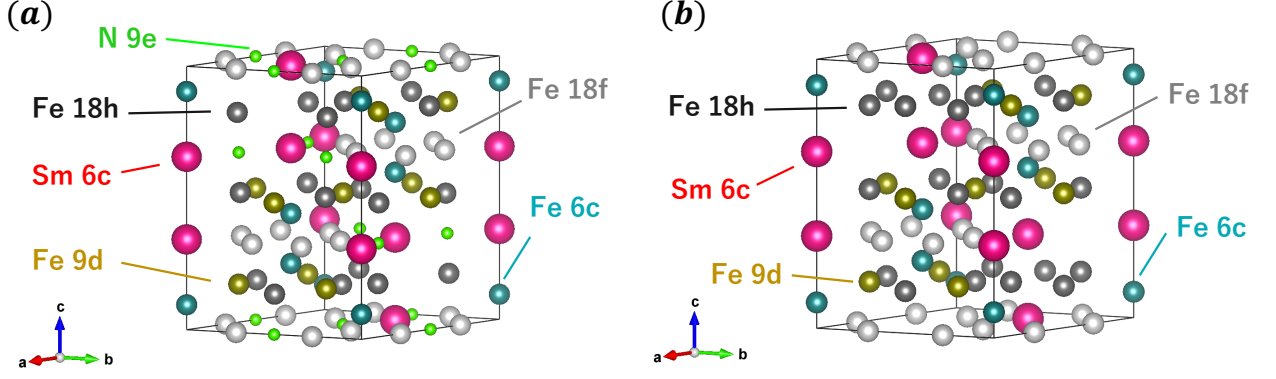


FIG. 1. Crystal structures of the hexagonal unit cell and non-equivalent atomic positions of (a)  $\text{Sm}_2\text{Fe}_{17}\text{N}_3$ <sup>22</sup> and (b)  $\text{Sm}_2\text{Fe}_{17}$ .<sup>28</sup>

TABLE IV. The crystal field parameters  $A_l^m \langle r^l \rangle$  [K] and the amplitude of the exchange mean-field  $|\mathbf{H}_m(0)|$  [K] computed using first-principles calculations, and the spin-orbit coupling constants  $\lambda$  [K] calculated from the experimental results<sup>29</sup>.

	Valency	$A_2^0 \langle r^2 \rangle$	$A_4^0 \langle r^4 \rangle$	$A_6^0 \langle r^6 \rangle$	$A_6^6 \langle r^6 \rangle$	$ \mathbf{H}_m(0) $	$\lambda$
$\text{Sm}_2\text{Fe}_{17}$	$\text{Sm}^{3+}$	-176.1	-18.27	-0.122	43.07	354.1	350
	$\text{Sm}^{2+}$	-8.07	-17.27	0.08	50.25	372.5	387
$\text{Sm}_2\text{Fe}_{17}\text{N}_3$	$\text{Sm}^{3+}$	-576.7	7.055	-1.213	29.85	176.3	350
	$\text{Sm}^{2+}$	-718.5	11.27	-1.142	28.54	150.5	387

are shown in FIG. 2 (b), in the same manner as FIG. 2 (a). The saturation magnetization is reduced as changing the valency from  $\text{Sm}^{3+}$  to  $\text{Sm}^{2+}$ ; however, the qualitative behavior of the curves does not change from FIG. 2 (a).

### C. Magnetization curves of $\text{Sm}_2\text{Fe}_{17}$

Next, we look at the magnetic properties of  $\text{Sm}_2\text{Fe}_{17}$  described by the effective spin model. FIG. 2 (c) shows the calculated magnetization curves along the hard and easy directions at  $T = 4.2\text{K}$ . We can clearly see that the magnetic anisotropy is qualitatively different between the systems with the trivalent  $\text{Sm}^{3+}$  and the divalent  $\text{Sm}^{2+}$  ions. When we assume the divalent  $\text{Sm}^{2+}$  configuration, the system shows planar anisotropy. Thus, the divalent results can reproduce the behavior that is experimentally observed<sup>1</sup>, as shown by a blue line in FIG. 2 (c) at 4.2K. We also show the curves at 300K in FIG. 2 (d). The qualitative behavior is almost the same as the results at 4.2K. It is noted that we can see the spin reorientation phenomenon. As stated in the Introduction, the orientation of the magnetization of this compound was experimentally found to deviate from the basal  $a$ - $b$  plane by as much as  $10^\circ$  at low temperatures<sup>1</sup>. Moreover, at room temperature, the spontaneous magnetization lies within the basal plane itself. In our results, for the divalent configuration,

when the external magnetic field is not applied, we cannot see the finite magnetization along the  $[001]$  direction at 4.2K; however, we can see the finite magnetization along the  $[001]$  direction at 300K. The divalent configuration results can qualitatively reproduce the magnetization curves for  $\text{Sm}_2\text{Fe}_{17}$ , but they cannot explain direction of the spontaneous magnetization at zero field. From our results, the curves assuming the divalent  $\text{Sm}^{2+}$  configuration can reproduce the experimental behaviors. However, as stated in the introduction, XAS experiments have shown that the Sm ions in  $\text{Sm}_2\text{Fe}_{17}\text{N}_x$  are trivalent  $\text{Sm}^{3+}$ . One possible reason for this discrepancy is the CFPs. The open core method is used in our calculations. The Sm ions are assumed to be in an atomic-like state in this method. The hybridization of 4f and other orbitals is not taken into account in our CFPs. One possible method beyond the open core method is the Wannierization proposed by Novák *et al.*<sup>30</sup> In this method, 4f electrons are treated as valence electrons and projected using localized Wannier functions. Thus, we can incorporate the hybridization of 4f and other orbitals in this method. If the hybridization is taken into account, the CFPs and the anisotropy might be changed.

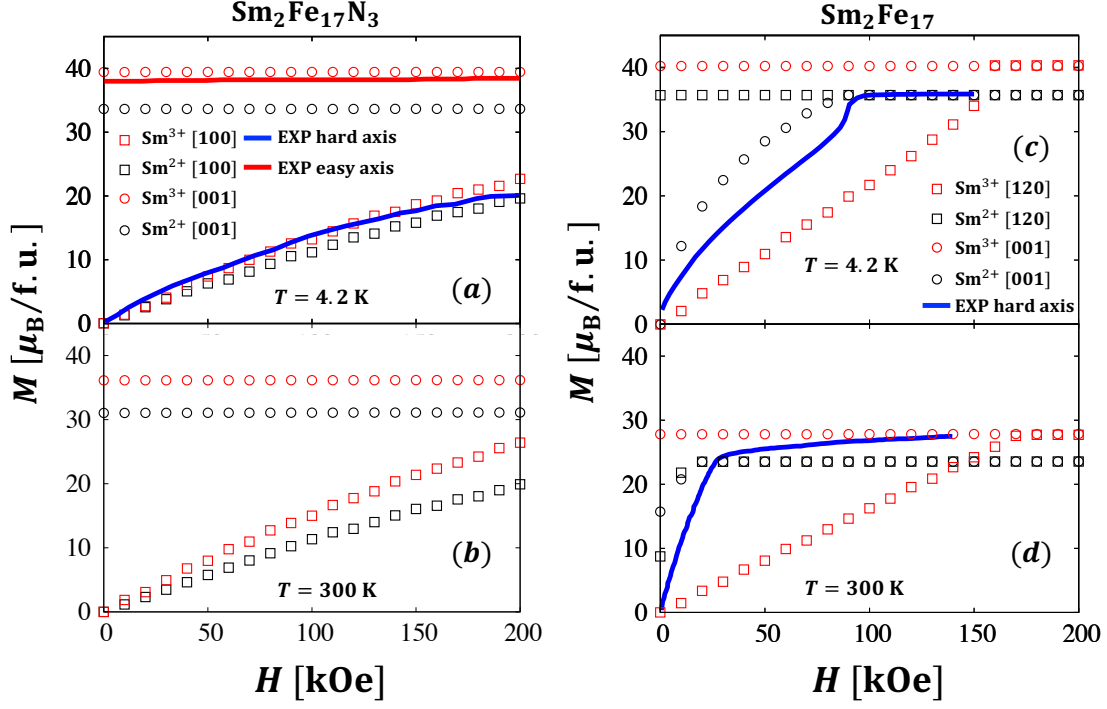


FIG. 2. The calculated magnetization curves of  $\text{Sm}_2\text{Fe}_{17}\text{N}_3$  at (a) 4.2K and (b) 300K and  $\text{Sm}_2\text{Fe}_{17}$  at (c) 4.2K and (d) 300K.  $\text{Sm}^{2+}$  and  $\text{Sm}^{3+}$  are indicated by black and red plots, respectively, where  $H$  [kOe] is the strength of the applied external magnetic field. In (a) and (b), the circles and squares indicate the results along the principal axis of [001] and [100] direction, respectively, and in (c) and (d), the circles and squares indicate the results along the principal axis of [001] and [120] direction, respectively. The experimental curves shown by red and blue lines in (a) at 4.2K are extracted from Koyama *et al.*<sup>25</sup>, in which the curves for 300K are not shown. The experimental curves in (c) and (d) at 4.2K and 300K are extracted from Diop *et al.*<sup>1</sup>

#### D. Anisotropy constants $K_1(T)$ and $K_2(T)$

We show the temperature dependence of the magnetic anisotropy constants  $K_1(T)$  and  $K_2(T)$  of  $\text{Sm}_2\text{Fe}_{17}\text{N}_3$  and  $\text{Sm}_2\text{Fe}_{17}$  in FIG. 3 (a) and (b), respectively. The anisotropy constants  $K_1(T)$  and  $K_2(T)$  of  $\text{Sm}_2\text{Fe}_{17}\text{N}_3$  shown in FIG. 3 (a) are always positive regardless of the valency of the Sm ions. The total anisotropy constants  $K_1(T)$  which include  $K_{\text{Fe}}$ , at 4.2K and 300K for each valency are indicated by triangles. The total anisotropy constants  $K_1(T)$  are positive at 4.2K and 300K and close to the values measured by Wirth *et al.*<sup>31</sup> at low temperature. This implies that  $\text{Sm}_2\text{Fe}_{17}\text{N}_3$  shows uniaxial anisotropy at any temperature. The temperature dependence of  $K_1(T)$  and  $K_2(T)$  of  $\text{Sm}_2\text{Fe}_{17}$  is shown in FIG. 3 (b). We can see that the calculation results with trivalent  $\text{Sm}^{3+}$  show positive  $K_1(T)$  and  $K_2(T)$  at any temperature. Therefore,  $\text{Sm}_2\text{Fe}_{17}$  with trivalent  $\text{Sm}^{3+}$  would show uniaxial anisotropy. In contrast, we can see negative  $K_1(T)$  in the results with divalent  $\text{Sm}^{2+}$  configuration. The total anisotropy constants are also shown in the same manner as  $\text{Sm}_2\text{Fe}_{17}\text{N}_3$  in FIG. 3 (a). Our total anisotropy constant for  $\text{Sm}^{2+}$  is close to the experimental values shown by Brennan *et al.*<sup>23</sup> and Isnard *et al.*<sup>32</sup> at low temperature. At 300K, our result is in good agree-

ment with the value measured by Isnard *et al.*<sup>32</sup>, where  $K_1$  is  $-1.75$  [MJ/m<sup>3</sup>] at 300K. Our total anisotropy constants  $K_1$  for  $\text{Sm}^{2+}$  are negative at 4.2K and 300K. This implies that  $\text{Sm}_2\text{Fe}_{17}$  with divalent  $\text{Sm}^{2+}$  would show planar anisotropy at low temperature. From the calculated anisotropy constants, the experimentally measured magnetization curve for  $\text{Sm}_2\text{Fe}_{17}\text{N}_3$  can be explained by both results; however, the curve for  $\text{Sm}_2\text{Fe}_{17}$  can be explained only by the divalent results.

#### IV. SUMMARY

In this work, we have calculated the magnetization curves and the temperature dependence of the anisotropy constants of  $\text{Sm}_2\text{Fe}_{17}$  and  $\text{Sm}_2\text{Fe}_{17}\text{N}_3$  by using the effective spin model based on first-principles calculations with the open core method. We showed that for  $\text{Sm}_2\text{Fe}_{17}\text{N}_3$  the curves generated by the  $\text{Sm}^{3+}$  model are in good agreement with the experimentally measured curves. The total anisotropy constants  $K_1(T)$  calculated for  $\text{Sm}_2\text{Fe}_{17}\text{N}_3$  assuming  $\text{Sm}^{3+}$  and  $\text{Sm}^{2+}$  qualitatively reproduce the experimentally measured behavior, with the results from  $\text{Sm}^{3+}$  close to the experimental value. In contrast, the results for  $\text{Sm}_2\text{Fe}_{17}$  assuming

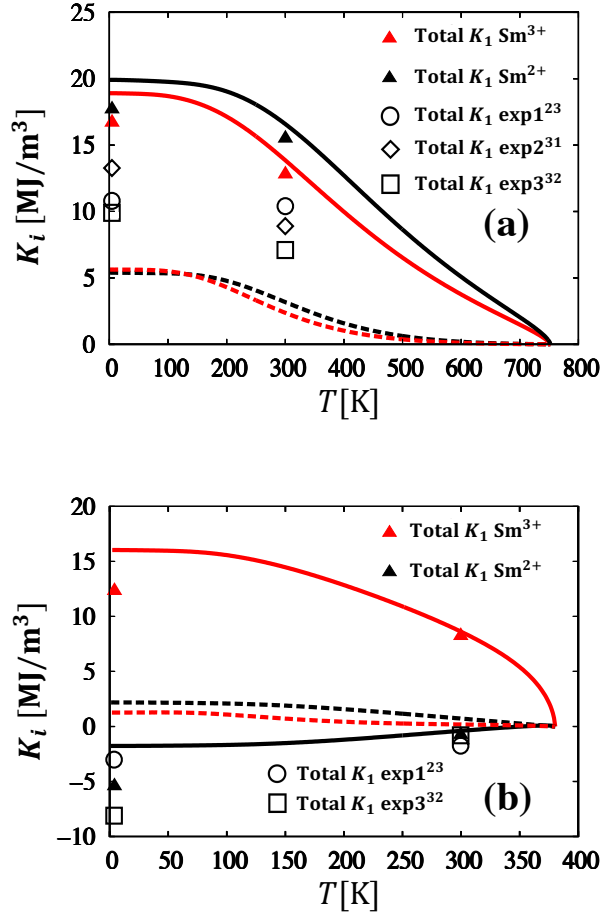


FIG. 3. The calculated magnetic anisotropy constants  $K_1$  (solid lines) and  $K_2$  (dashed lines) per two Sm ions in (a)  $\text{Sm}_2\text{Fe}_{17}\text{N}_3$  and (b)  $\text{Sm}_2\text{Fe}_{17}$  with  $\text{Sm}^{3+}$  (red lines) or  $\text{Sm}^{2+}$  (black lines) electronic configuration. The total anisotropy constants  $K_1$  with Fe sublattice contribution  $K_{\text{Fe}}$  are indicated by red ( $\text{Sm}^{3+}$ ) and black ( $\text{Sm}^{2+}$ ) triangles. The open shapes indicate the experimentally measured values of  $K_1$ ; the open circles correspond to the values of Brennan *et al.*<sup>23</sup>, the open squares correspond to the values of Isnard *et al.*<sup>32</sup>, and the open diamonds correspond to the values of Wirth *et al.*<sup>31</sup>

$\text{Sm}^{2+}$  are consistent with the experimentally measured curves. In addition, the temperature dependence of the total anisotropy constants for  $\text{Sm}^{2+}$  is consistent with experimentally observed behavior. However, previously reported XAS experiments<sup>10</sup> have found that the Sm ions in  $\text{Sm}_2\text{Fe}_{17}\text{N}_x$  are trivalent configuration regardless of the nitrogen content  $x$ .

It is noted that the effective spin model based on DFT calculations with the open core method might not be able to describe the magnetic properties of  $\text{Sm}_2\text{Fe}_{17}$ . One possible reason for this disagreement is that the hybridization effects between the 4f orbitals of the Sm ions and other orbitals cannot be included in the CFPs by using the open core method. In the open core method, 4f orbitals are treated as atomic-like core states and the valence effects of them are completely neglected. Taking the valence effects into account might change the CFPs and the magnetic anisotropy of the systems. For more precise investigation, further research should apply a more realistic method, such as the Wannierization method,<sup>30,33</sup> that can incorporate the hybridization effects of 4f electrons and other orbitals to evaluate the CFPs.

## ACKNOWLEDGMENTS

This work was partially supported by ESICMM Grant Number 12016013, and ESICMM is funded by the Ministry of Education, Culture, Sports, Science and Technology (MEXT). S. Y. acknowledges support from GP-Spin at Tohoku University, Japan. Work of T. Y. was supported by JPS KAKENHI Grant Number JP18K04678. Work of P. N. was supported by project SOLID21. Part of the numerical computations were carried out at the Cyberscience Center, Tohoku University, Japan.

- <sup>1</sup> L. V. B. Diop, M. D. Kuz'min, K. P. Skokov, D. Yu. Karpenkov, and O. Gutfleisch, *Phys. Rev. B* **94**, 144413 (2016).
- <sup>2</sup> B. I. Min, J.-S. Kang, J. H. Hong, S. W. Jung, J. I. Jeong, Y. P. Lee, S. D. Choi, W. Y. Lee, C. J. Yang, and C. G. Olson, *J. Phys.: Condens. Matter* **5**, 6911 (1993).
- <sup>3</sup> L. Steinbeck, M. Richter, U. Nitzsche, and H. Eschrig, *Phys. Rev. B* **53**, 7111 (1996).
- <sup>4</sup> Yu. V. Knyazev, Yu. I. Kuz'min, A. G. Kuchin, A. V. Lukoyanov, and I. A. Nekrasov, *J. Phys.: Condens. Matter*

- 19**, 116215 (2007).
- <sup>5</sup> T. Pandey, M.-H. Du, and D. S. Parker, *Phys. Rev. Appl.* **9**, 034002 (2018).
- <sup>6</sup> K. Buschow, *Rep. Prog. Phys.* **54**, 1123 (1991).
- <sup>7</sup> D. McNeely and H. Oesterreicher, *J. Less-Common Met.* **44**, 183 (1976).
- <sup>8</sup> M. Ogura, A. Mashiyama, and H. Akai, *J. Phys. Soc. Jpn.* **84**, 084702 (2015).
- <sup>9</sup> X. C. Kou, F. R. de Boer, R. Grössinger, G. Wiesinger, H. Suzuki, H. Kitazawa, T. Takamasu, and G. Kido, *J. Magn.*

- Magn. Mater. **177–181**, 1002 (1998).
- <sup>10</sup> T. W. Capehart, R. K. Mishra, and F. E. Pinkerton, Appl. Phys. Lett. **58**, 1395 (1991).
  - <sup>11</sup> H. W. de Wijn, A. M. van Diepen, and K. H. J. Buschow, Phys. Rev. B **7**, 524 (1973).
  - <sup>12</sup> S. G. Sankar, V. U. S. Rao, E. Segal, W. E. Wallace, W. G. D. Frederick, and H. J. Garrett, Phys. Rev. B **11**, 435 (1975).
  - <sup>13</sup> M. Yamada, H. Kato, H. Yamamoto, and Y. Nakagawa, Phys. Rev. B **38**, 620 (1988).
  - <sup>14</sup> M. Richter J. Phys. D: Appl. Phys. **31** 1017 (1998).
  - <sup>15</sup> J. Franse and R. Radwański, in *Handbook of Magnetic Materials*, edited by K. H. J. Buschow (North-Holland, Amsterdam, 1993), Vol. 7.
  - <sup>16</sup> T. Yoshioka, and H. Tsuchiura, Appl. Phys. Lett. **112**, 162405 (2018).
  - <sup>17</sup> T. Yoshioka, H. Tsuchiura, and P. Novák, Phys. Rev. B **102**, 184410 (2020).
  - <sup>18</sup> P. Novák, Phys. Stat. Sol. B **198**, 729 (1996).
  - <sup>19</sup> M. Diviš, K. Schwarz, P. Blaha, G. Hilsher, H. Michor, and S. Khmelevskiy, Phys. Rev. B **62**, 6774 (2000).
  - <sup>20</sup> M. Diviš, J. Ruzs, H. Michor, G. Hilsher, P. Blaha, and K. Schwarz, J. Alloys Compd. **403**, 29 (2005).
  - <sup>21</sup> P. Blaha, K. Schwarz, G. K. H. Madsen, D. Kvasnicka, and J. Luitz, *WIEN2k, An Augmented Plane Wave + Local Orbitals Program for Calculating Crystal Properties* (Karlheinz Schwarz, TU Wien, Austria, 2001).
  - <sup>22</sup> N. Inami, Y. Takeuchi, T. Koide, T. Iriyama, M. Yamada and Y. Nakagawa, J. Appl. Phys. **115**, 17A712 (2014).
  - <sup>23</sup> S. Brennan, R. Skomski, O. Cugat and J. M. D. Coey, J. Magn. Magn. Mater. **140–144**, 971 (1995).
  - <sup>24</sup> M. D. Kuz'min, Phys. Rev. Lett. **94**, 107204 (2005).
  - <sup>25</sup> K. Koyama and H. Fujii, Phys. Rev. B **61**, 9475 (2000).
  - <sup>26</sup> R. Sasaki, D. Miura, and A. Sakuma Appl. Phys. Express **8**, 043004 (2015).
  - <sup>27</sup> M. S. S. Brooks, L. Nördstrom, and B. Johansson, J. Phys. Condens. Matter **3**, (1991).
  - <sup>28</sup> A. Teresiak, M. Kubis, N. Mattern, K.-H. Müller, and B. Wolf, J. Alloys Compd. **319**, 168 (2001).
  - <sup>29</sup> D. S. McClure, Solid State Phys. **9**, 399–525 (1959).
  - <sup>30</sup> P. Novák, K. Knížek, and J. Kuneš, Phys. Rev. B **87**, 205139 (2013).
  - <sup>31</sup> S. Wirth, M. Wolf, K.-H. Müller, R. Skomski, S. Brennan, and J. M. D. Coey, IEEE Trans. Magn. **32**, 4746 (1996).
  - <sup>32</sup> O. Isnard, S. Miraglia, M. Guillot, and D. Fruchart, J. Appl. Phys. **75**, 5988 (1994).
  - <sup>33</sup> T. Yoshioka, H. Tsuchiura, and P. Novák, Mater. Res. Innov. **19**, S3 (2015).